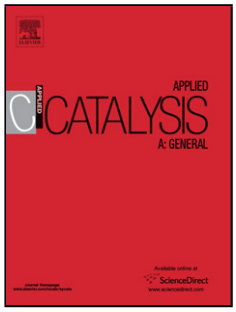

Title: Nickel-Promoted Copper-Silica Nanocomposite Catalysts for Hydrogenation of Levulinic Acid to Lactones using formic acid as a hydrogen feeder

Author: Pravin P. Upare Myung-Geun Jeong Young Kyu Hwang Dae Han Kim Young Dok Kim Dong Won Hwang U.-Hwang Lee Jong-San Chang

PII: S0926-860X(14)00758-3
DOI: http://dx.doi.org/doi:10.1016/j.apcata.2014.12.007
Reference: APCATA 15145

To appear in: *Applied Catalysis A: General*

Received date: 16-5-2014
Revised date: 28-11-2014
Accepted date: 2-12-2014

Please cite this article as: P.P. Upare, M.-G. Jeong, Y.K. Hwang, D.H. Kim, Y.D. Kim, D.W. Hwang, U.-H. Lee, J.-S. Chang, Nickel-Promoted Copper-Silica Nanocomposite Catalysts for Hydrogenation of Levulinic Acid to Lactones using formic acid as a hydrogen feeder, *Applied Catalysis A, General* (2014), http://dx.doi.org/10.1016/j.apcata.2014.12.007

Nickel-Promoted Copper-Silica Nanocomposite Catalysts for Hydrogenation of Levulinic Acid to Lactones using formic acid as a hydrogen feeder

Pravin P. Upare, [a] *Myung-Geun Jeong,* [a,b] *Young Kyu Hwang,* *[a,c] *Dae Han Kim,* [b] *Young Dok Kim,* [a,b] *Dong Won Hwang,* [a,c] *U-Hwang Lee,* [a] *and Jong-San Chang* *[a,b]

[a] *Catalysis Center for Molecular Engineering, Korea Research Institute of Chemical Technology (KRICT), 141 Gajeong-Ro, Yuesong, Daejeon 305-600, Korea, Fax: (+) 82-42-860-7676,*
E-mail: ykhwang@krict.re.kr and jschang@krict.re.kr

[b] Department of Chemistry, Sungkyunkwan University, Suwon 440-476, Korea *E-mail: jschang020@skku.edu*

[c] *Department of Green Chemistry, University of Science and Technology (UST),217 Gajeong-Ro, Yuseong, Daejeon 305-350, Korea*

Abstract

Highly active, thermally stable nickel-promoted copper-silica nanocomposite catalysts were prepared via a deposition-precipitation method and used for hydrogenation of levulinic acid (LA) using formic acid (FA) as H_2 feeder. Ni(20)Cu(60)-SiO_2 (3:1 weight ratio of Cu to Ni, 80 wt% metal content) showed better activity for vapor-phase formation of γ-valerolactone (GVL) from LA with FA as a hydrogen source. The catalyst selectively converts 99% of LA into 96% of GVL; the remaining 4% is angelica-lactone (AL). The effect of different concentrations of Ni promoted on Cu-silica and different LA to FA molar ratios on the catalyst activity affecting the hydrogen-free hydrogenation of LA was studied. The catalyst Ni(20)Cu(60)-SiO_2 exhibited long-term stability (200 h) without loss in activity. Characterization using TEM, XPS, TPR, XRD, and N_2O titration was performed to find the most active phase for LA hydrogenation to GVL and the reason for the long-term stability. It was found that Ni-promoted well-dispersed metallic Cu species were the most active phases in hydrogenation, and the nanocomposite nature of the catalyst helped in providing long-term stability to the active phase.

Keywords: γ-valerolactone • Levulinic acid • Hydrogenation • Formic acid • Nickel-promoted copper on silica

1. Introduction

For over half a century, most chemical industries have depended on fossil resources for major feed stocks; however, most of the fossil-fuel reservoirs are in the mature stages of their economic life spans. Hence, it is crucial to develop integrated systems that can produce valuable chemicals from alternative biomass [1-4]. Safe and economic production of bio-based chemicals and biofuels is a major challenge of today [1-4]. Among the bio-based chemicals, levulinic acid (LA) is a well-known product developed by the hydrolysis of hexoses (six-carbon sugars, C6 sugars), and it can be obtained inexpensively from the decomposition of cellulosic materials [3]. Alternatively, formic acid (FA) may be coproduced with LA via acid-catalyzed conversion of C6 sugars [4]. Very recently, Upare *et al*. successfully demonstrated the Brønsted-acid-catalyzed chemical conversion of C6 sugars and cellulose to LA [4a]. Consequently, LA is an attractive starting material for the production of many useful C5-based compounds such as γ-valerolactone (GVL), 2-methyltetrahydrofuran (MTHF), and other derivatives. GVL can be utilized as a versatile platform chemical for various valuable products [5]; it is also useful in the industry as a solvent for lacquers, insecticides, and adhesives. It also has some uses in cutting oil, brake fluid, and as a coupling agent in dye baths [5].

Recently, Dumesic *et al.* reported an integrated process for the production of liquid alkenes from GVL and suggested an inexpensive method to produce GVL from biomass [6]. Catalytic approaches to the hydrogenation of LA to form GVL have been reported in the literature [3, 7, 8]. Most researchers used batch-type reactors and high-pressure hydrogen [3, 7] or supercritical CO_2 for their studies [8]. Recently, Fu *et al.* reported an economically viable hydrogen-free (H_2-free) synthesis of GVL from LA, using FA as a hydrogen source, in a batch-type reactor over ruthenium-based homogenous and heterogeneous catalytic systems [9]. They also reported the selective synthesis of LA and FA in a molar ratio of approximately 1:1.

There are a few recent reports involving the use of heterogeneous catalysts for the direct synthesis of GVL from LA and FA as a hydrogen source using gold [10] and ruthenium-based catalysts [9-11]. Very recently, Dumesic *et al*. reported the continuous production of GVL from LA and FA using H_2SO_4 over a noble-metal-supported catalyst at 35 bar [12]. It is worthwhile to mention that continuous vapor-phase processes have advantages over batch-type processes, such as easy recovery of both the catalyst and products. As reported elsewhere, the noble metals Ru, Pt, and Pd are frequently considered good

hydrogenation catalysts at high temperatures [7]. Transitions metals can also be utilized as catalysts for hydrogenation [13]. However, copper and nickel are rarely considered effective hydrogenation catalysts at high temperatures because of their leaching in the liquid phase and sintering of copper particles at high temperatures [14]. Recently, Upare *et al*. reported which provide a sustainable catalyst life in a continuous hydrocyclization of biomass-derived carboxylic acids to corresponding hydrofurans and lactones under vapor-phase conditions in hydrogen [15]. The nanocomposite nature of copper-silica catalysts helps in preventing metallic sintering and in avoiding significant deactivation. Therefore, it seemed worthwhile to investigate the evolution of the active metal surface in catalysts. Herein, we report a continuous process for selective synthesis of GVL from LA using FA as a hydrogen source over an inexpensive highly stable Ni-promoted Cu-SiO_2 nanocomposite catalyst system under atmospheric pressure. Scheme 1 represents the continuous production of GVL from biomass via hydrogenation of LA using FA as a hydrogen source.

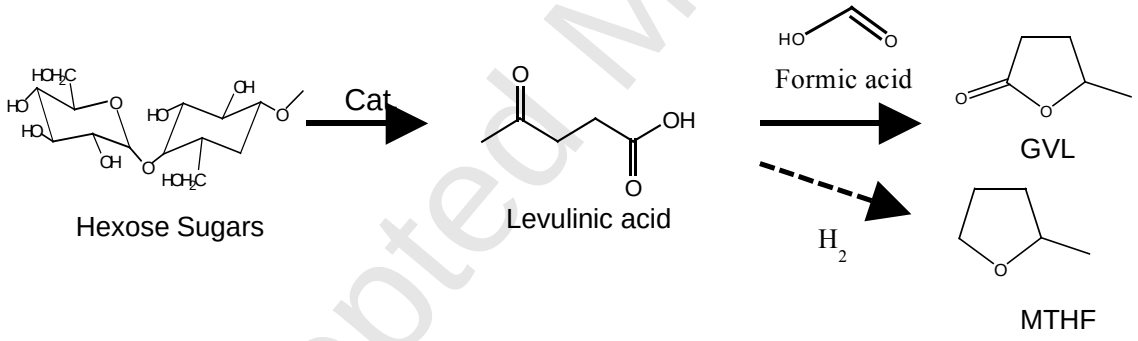

Scheme 1. Synthesis of lactones from biomass-derived levulinic acid and formic acid.

2. Experimental Section

2.1. Materials

$Cu(NO_3)_2 \cdot 3H_2O$ and $Ni(NO_3)_2 \cdot 6H_2O$ were supplied by Wako, and NaOH (AR grade) was obtained from local suppliers at Daejeon, South Korea, and were used as received. The SiO_2 source was Ludox SM-30 colloidal silica supplied by Aldrich. It had a surface area of 345 $m^2\ g^{-1}$ and was used as received. LA (98%, Alfa Aser), FA (99%, Aldrich), and 1,4-dioxane (99.5%, Alfa Aser) were used for hydrogenation of LA to GVL.

2.2. Catalyst preparation

In a typical catalyst-preparation procedure, known amounts of $Cu(NO_3)_2 \cdot 3H_2O$ and $Ni(NO_3)_2 \cdot 6H_2O$ are dissolved in doubled-distilled water, and the desired amount of silica solution (Ludox SM-30, S_{BET} = 345 $m^2 g^{-1}$) comprising 7-nm silica nanoparticles was added dropwise to the water at 4 °C. For precipitation, a solution of 0.1-N NaOH was added to the above suspension until the pH became 9.2. The suspension was then stirred for 12 h at room temperature, followed by stirring at 85 °C for 5 h. The resulting suspension was filtered and washed with distilled water repeatedly until sodium was no longer detected in the filtrate. The solid was then dried in air at 120 °C for 12 h, pressed into pellets, crushed, sieved (No. 20–40 mesh), and finally calcined in air at 600 °C for 8 h. Before the reaction, catalyst samples were reduced at 290 °C with a mixture of 5% H_2 in N_2 (30 ml/min) for 2 h. The metal composition with silica will be described hereinafter as Ni(x)Cu(y)-SiO_2, x + y = 80 wt% based on metal oxides, NiO and CuO. Prior to the characterization of catalysts, the reduced and used materials were stabilized in N_2 atmosphere after their reduction at 290 ^oC or after reaction at 265 ^oC, by which we could somehow able to prevent the significant oxidation of reduced metallic species before characterizations of catalysts.

2.3. Catalyst characterization

The structure and crystallinity of the catalyst samples were determined by X-ray diffraction analysis on Rigaku Ultima IV Diffractometer (40KV, 40mA), which is equipped with Cu tube in Graphite-Monochromatic for Cu Kα radiation. XRD results were recorded by using PDXL software program in the 2 theta range between 5^o to 80^o using slower 1^o per min scanning rate. H_2-TPR experiments were carried out in Micromeritics model Pulse Chemisorb 2705 equipped with a thermal conductivity detector (TCD) to monitor H_2 consumption is in the temperature range of 100 ^oC to 800 ^oC in 5%H_2/He. XPS analysis of the catalysts was carried out to identify the chemical state of the surfaces before and after reduction. The XPS system consisted of a preparation and main chamber, connected via a gate valve. Reduced catalysts were treated under 1 atm of 5% H_2/N_2 at 350 ^oC for 4h. The reduction step was advanced into the preparation chamber, and then XPS spectra of each catalyst were obtained in the main chamber (base pressure ~3.0 × 10^{-10} Torr) without exposing the samples to air. XPS spectra were collected using Mg Kα (1253.6 eV) as a monochromatic energy source and with a concentric hemispherical analyzer (CHA,

PHOIBOS-Has 2500, SPECS). Charging effects were calibrated with Ag $3d_{5/2}$ (368.3 eV) and $3d_{3/2}$ (374.3 eV) spectra. For detailed analysis, Cu and Ni $2p_{3/2}$ spectra were deconvoluted using CASA-XPS software. Background subtraction was processed by Shireley method. Each spectrum was fitted with a linearly combined Gaussian/Lorenzian functions. Specific surface areas of catalysts were measured by N_2 physisorption at liquid nitrogen temperature using Micromeritics Tristar 3000 surface area analyzer and standard multipoint BET analysis method. Samples were degassed in flowing N_2 for 12 h at 200 °C before N_2 physisorption measurements. The specific surface areas were evaluated using the Brunauer-Emmett-Teller (BET) method in the p/p_0 range of 0.05-0.2. The particle morphology and crystal size of catalysts were examined using a transmission electron microscope (TEM; Technai G2 Retrofit). Samples for TEM analysis were prepared by suspending the catalyst particles in ethyl alcohol and mounting them on carbon-filmed copper grids.

2.4. Levulinic acid hydrogenation

The hydrogenation of LA with FA was performed in a conventional stainless-steel fixed-bed reactor (internal diameter 1 cm and length 300 mm), in which 1 g of catalyst was packed. Vaporized mixtures of LA and FA dissolved in 1,4-dioxane (10 wt.% = 7.2g of LA and 2.85 g of FA in 90 g of 1,4-dioxane) were introduced into the reactor via a syringe pump with 20 mL/min of nitrogen flow through a preheated line. In order to study the effect of FA concentration, we keep constant weight of LA (7.2 g) and concentration of FA was varied accordingly. The liquid products were analyzed using a gas chromatograph (DONAM DS6200) equipped with a flame ionization detector and capillary column (CycloSil-B). Only the molar conversion of LA was considered for this study because FA was used as a hydrogen source. The decomposition of FA to form H_2 and CO_2 was confirmed using GC equipped with a TCD detector with a Carbosphere column.

3. Results and Discussion

3.1. Catalyst characterization results

3.1.1. XRD analysis of catalysts

The XRD patterns of the NiCu-SiO_2 catalysts with different metallic loading are shown in Figure 1. The peak position on XRD patterns of the catalysts were conformed from the reference JCPDS cards (NiO from no. 47-1049, CuO from no. 41-0254 and Cu_2O from no.

71-3645). On the XRD pattern of calcined catalysts, we could clearly see the oxide phases of nickel (NiO 2θ at 37.25^o, 43.29^o and 62.86^o) and copper (CuO at 35.44^o, 38.73^o, 48.73^o, 53.47^o, 61.55^o and Cu_2O at 36.43^o, respectively). Presence of CuO and NiO peaks at their reference position without any shifting on the XRD pattern of calcined catalysts (Figure 1) clearly indicates the absence of solid solution between CuO and NiO in catalysts [17]. The XRD peaks of the NiO were also observed in the case of reduced and used Cu-Ni catalysts (Figure 2 and 3).

The diffraction peaks for metallic Cu were observed in the XRD patterns of both reduced and used catalysts (Figure 2 and 3). The diffraction peaks at 2θ of 43.30°, 50.44°, and 74.13° (JCPDS card no.4-0836) are the characteristic peaks corresponding to the (111), (200), and (220) planes of metallic Cu, and the peaks at 2θ of 44.51°, 51.85°, and 76.37° (JCPDS card no.4-0850) are the characteristic peaks for metallic Ni corresponding to the same (111), (200), and (220) lattice planes of metallic Cu, respectively [15,16]. However, the characteristic diffraction peaks related to nickel phases were difficult to observe, presumably because of the high dispersion of metallic nanoparticles and the similarity of their 2θ peak positions with that of metallic Cu in the XRD profiles of the NiCu-SiO_2 catalysts. Even for the 20% to 40% Ni-loaded catalysts, the XRD peak for Ni was not seen clearly because of the high resistance of nickel oxide for sintering under reduction condition at at 290 ^{o}C for 2h [13]. This also means that Ni-promoted catalysts existed with some metallic Ni moieties along with NiO in the fixed bed reactor during hydrogenation, which can also help to enhance the ability of copper for selective hydrogenation of LA to GVL and also improved the stability of the catalysts. When the Ni(80)/SiO_2 catalyst was reduced at 290 ^{o}C, we could see the reduced Ni species. However, all catalysts showed only a characteristic metallic Cu peak in the XRD patterns, which suggests that there was less possibility to form solid solution between metallic Cu and Ni [16]. As per XRD patterns and recent reference [17], this is the not an indication for existences of Cu-Ni solid solution in the synthesized materials.

The metallic particles are finely dispersed on the silica and played an important role in enhancing the catalytic activity in the vapor-phase hydrogenation of biomass-derived LA. The average particle sizes of the metallic Cu particles were calculated by using Scherrer equation using FWHM values. Particle size of Cu dramatically decreased with the increasing of nickel amount in the Cu-Ni catalyst, and it is estimated to be around 23 nm, 19 nm, 7nm, 6 nm and 4.3 nm for the nickel with 0 to 40% loading, respectively. Very fine particles of NiO (1.7 to 2 nm) were observed in the case of Ni with 80% of loading (Ni(80)/SiO_2). After LA

hydrogenation, the diffraction peaks of the metallic Cu remained almost the same for the Nickel with 8% and 20% loading, even after 200 h of hydrogenation. This is consistent well with the TEM results.

3.1.2. TEM analysis of catalysts

The TEM and HR-TEM images for the reduced and used catalysts are presented in Figure 4. The HR-TEM images of the Ni(8)Cu(72)-SiO_2 and Ni(20)Cu(60)-SiO_2 catalysts (Figure 4) show that metallic nanoparticles exist in the ellipsoid shapes of (111) or (100) faces [18], and it is clearly shown in the HR-TEM image (Figure 4e) of Ni(8)Cu(72)-SiO_2 catalyst. Homogenous dispersion of metallic nanoparticles is clearly seen in the TEM images of both catalysts; these results correlate with the H_2-chemisorption results (Table 1). The average size of the metal particles was determined by measuring the projected areas of individual particles in the TEM images and calculating the equivalent diameter. This corresponds to the diameter of a circle with the same area and was found to be 17–19 nm for Ni(8)Cu(72)-SiO_2 and 5–9 nm for Ni(20)Cu(60)-SiO_2 reduced catalysts. The particle size increased to 20–22 nm in the used catalysts (after 200 h of reaction time) because of slight sintering of metallic nanoparticles at higher reaction temperatures. However, this did not significantly reduce the activity of the catalysts. This was proven with the time-on-stream results. More interestingly, even the specific morphology of both catalysts did not change much, even after a long reaction time (Figure 4). This means that these catalysts exhibit long-term stability and can be reused several times for hydrogenation reactions. It was very difficult to determine the state of existence of the nickel in the catalyst after reduction by TEM analysis because of its electromagnetic nature. Although we are not sure about the nickel species (in terms of nickel oxide or copper-nickel alloy), data from other characterization techniques (i.e., TPR, H_2-chemisorption, and XPS) clearly showed that the nickel species are highly dispersed on the support, and they interact strongly with the support and Cu. The TEM-EDS mapping images for each metal in a selected area of the Ni(20)Cu(60)-SiO_2 catalyst are presented in Figure 5. The TEM-EDS analysis clearly shows the homogenous dispersion of metallic Cu and Ni nanoparticles on the support. The EDS of Ni(20)Cu(60)-SiO_2 catalyst are shown in Figure 5. From these, the amount of atomic loading and their distribution were clearly obtained. The metallic loading was also confirmed through the EDS analysis, and these results matched those from the ICP analysis. The TEM and TEM-EDS mapping analyses confirmed that the copper and nickel species are homogenously

dispersed in the catalyst. These results also indicate that silica nanoparticles in the low silica-loaded catalysts can be used as an inorganic matrix to enhance homogeneous dispersion of high content metals instead of catalyst support. No evidence was obtained for the presence of copper-nickel alloy in the catalyst.

3.1.3. XPS and TPR analyses of catalysts

Tables 2 and 3 present the atomic content of the bulk and surfaces of various catalysts, as determined by ICP and XPS, respectively. The ICP data (Table 2) indicate that the Cu ratio decreased with increased Ni loading, whereas the Si content was nearly constant as a function of Ni loading. In contrast, the XPS data (Table 3) show that increasing the Ni ratio decreased the Si ratio, whereas the Cu ratio on the catalyst surfaces was almost constant. No significant change was observed in the atomic ratios on the catalyst surfaces before and after reduction.

Figure 6 shows the Cu 2p and Ni 2p XPS spectra of the calcined and reduced catalysts. In Figure 6 (a), the Cu $2p_{3/2}$ states of the calcined catalysts show two peaks centered at 934.1 eV and 935 eV, which can be attributed to CuO and $Cu(OH)_2$, respectively [17, 19, 20]. In addition, the satellite peaks were observed at higher binding energy of ~ 9 eV than that of Cu $2p_{3/2}$ and $2p_{1/2}$. According to the references, the satellite of Cu 2p was typically in Cu^{2+} species, which is well-known shake-up satellite peak, not Cu^{2+} and metallic Cu species [17, 19, 20]. The shape of Cu 2p for calcined catalysts was shown similar regardless of the Ni-loading, indicating that Ni content didn't affect almost states of Cu species before reduction. The Ni $2p_{3/2}$ spectra presents two Ni states at 855.5 and 856.5 eV, which correspond to binding energy of Ni^{2+} oxides species such as $Ni(OH)_2$ and nickel silicates ($NiSiO_3$). Also, the presence of shake-up satellites, which were attributed to a multiple electron excitation, could be evidence supporting to that the oxidation states of Ni in calcined catalysts is +2 [20-22].

For a reduced Cu-SiO_2 catalyst (Figure 6 (c) and (d)), the Cu $2p_{3/2}$ state show a pronounced peak at 932.6 eV. It is ambiguous to distinguish oxidation state of Cu species according to binding energy [17, 19, 20]. Cu^{2+} could be characterized from metallic copper and Cu^{1+} by satellite peak. Comparing before reduction, the peak for satellite of Cu 2p was almost disappeared, even if the intensity in Ni(20)Cu(60)-SiO_2 sample remained slightly (as shown in inset). Also, the Auger parameter, which is defined as sum of the kinetic energy of Cu LMM transition and the binding energy of Cu $2p_{3/2}$ can provide clue to distinguish between Cu^{1+} and Cu^0 [17, 19, 20]. Auger parameter for three catalysts is equal to 1851.4 eV,

which is typical value of metallic copper. Thus, we can infer that the main state of copper in reduced catalysts is Cu^0. Moreover, a little intensity of satellite in Ni(20)Cu(60)-SiO_2 means existence of Cu^{2+} state, indicating the presence of Ni suppressed the reduction of $Cu(OH)_2$ and CuO to metallic Cu upon thermal treatment under H_2. This result is in line with the TPR data shown in Figure 5. Here, the reduction temperature of Cu increased with increasing Ni content. From the H_2-chemisorption data, it was observed that H_2 uptake increased with nickel loading (Table 1). A significant difference was observed in H_2 uptake with and without nickel catalyst: higher H_2 uptake occurred with the Ni-loaded catalysts, particularly much higher at Ni(40)Cu(40)-SiO_2. Ni $2p_{3/2}$ spectra of reduced catalysts appeared additional peak centered at 852.7 eV, which assigned to metallic nickel. This result is accordance with XRD pattern, though there are some difference in relative ratio of metallic Ni between bulk and surface. However, the main component of nickel was still silicate form. In Si 2p spectra of Ni(20)Cu(60)-SiO_2, the presence of shoulder at lower binding energy than main peak (104.5 eV) is in accordance with the result of Ni spectra [22] (SI supporting).

The TPR profile calcined catalysts are presented in Figure 7. The catalyst Cu(80)-SiO_2 showed the reduction peak for copper centered at 245 °C, and which gets shifted toward the higher temperature with the addition of nickel, which might result from strong interaction between copper and nickel [13, 23]. The reduction peaks of 20% loading to 40% loading are much shifted to the 269 ^oC and they are broader as compare to the nickel with zero and 8% loading. These boarder reduction peaks are seems to be merging of two reduction peaks due to reduction of CuO and bulk or surface NiO species. As per literature, lower temperature reduction of NiO is possible if they are free or weekly associated with the supports [13, 24]. Yin *et al.* [13] have also observed significant decreased the reduction temperature (lower than 297 ^oC) of nickel species due to the existence of copper. This result is also in agreement with the reported result [25]. The reduction peaks for nickel has been observed at 490^oC and 592 ^oC (as shown in inset of Figure 7) because nickel oxide was well dispersed and strongly interacted with Cu-silica [13, 17, 23, 24]. For comparison, we have also showed the reduction profile of Ni(80)/SiO_2 material in Figure 7(f). On which, three reduction peaks are centered at 314 ^oC, 490 ^oC and 295 ^oC are displayed. Lower reductions peaks is due to the reduction of bulk or surface nanosized NiO species and higher temperature reduction because of its well dispersion and strong interaction of NiO with support [24]. TPR results represent that Cu and Ni species are well dispersed on the silica support with their strong interaction with each

other. This is consistence with that the TEM data (Figure 2) clearly show that the Ni and Cu species are homogenously dispersed with silica nanoparticles.

3.2 Catalytic results of LA hydrogenation

3.2.1. Effect of variation in Ni and Cu loading

The Ni-promoted nanocomposite Cu-SiO_2 catalysts were prepared by deposition co-precipitation method. Details of catalyst preparation are given in the experimental section and in another paper [15]. The same procedure has been used for the preparation of 10Cu- and Cu(80)-SiO_2. Initially, we performed vapor-phase hydrogenation of LA over Cu(10)-SiO_2 at 265°C at atmospheric pressure and in a nitrogen flow with 1:1 molar ratio of LA and FA. The catalytic results for LA hydrogenation by silica catalysts with different Cu and Ni concentrations are presented in Table 4. Only 10% of the Cu on the silica converts 66% of LA into 55% angelica-lactone (AL) and 45% GVL. To increase the LA conversion, hydrogenation with a higher loading of Cu on silica (i.e., 80 wt.% Cu-SiO_2) was performed. The Cu(80)-SiO_2 catalyst produced 81% GVL and 19% AL with 83% conversion of LA. To enhance the LA conversion and GVL selectivity, we introduced a Ni-promoted Cu-SiO_2 nanocomposite catalyst in the reactor. The use of Ni has been well promoted for hydrogenation and hydrolysis [26]. In the LA hydrogenation, the Ni-promoted Cu-SiO_2 catalyst increased the LA conversion as well as GVL selectivity. Recently, we reported a higher activity of the NiCu-SiO_2 nanocomposite catalyst for direct hydrogenation of LA with H_2 to form 2-methyltetrahydrofuran (MTHF), wherein the catalyst was very active and stable for 320 h without significant loss in its activity [15].

Ni and Cu loadings on SiO_2 catalyst at different concentrations were tested. A marginal difference in the LA conversion and GVL selectivity was observed for Ni(4)Cu(76)-SiO_2. The Ni(4)Cu(76)-SiO_2 catalyst converted 85% of LA into 82% GVL and 18% AL remained. This means that 4% Ni was not very effective for increasing the GVL selectivity in LA hydrogenation of LA. In contrast, for 8% Ni loading Ni(8)Cu(72)-SiO_2, the LA conversion (88%) and GVL selectivity (88%) were higher and 12% AL remained. The Ni(20)Cu(60)-SiO_2 catalyst provides excellent catalytic activity and longer stability for hydrogenation of LA and has a high selectively for GVL. The maximum LA conversion of 98% and GVL selectivity of 92% were obtained with 20% nickel under the reaction conditions presented in Table 4. The higher nickel concentration above 20% of Ni (i.e., Ni(40)Cu(40)-SiO_2) did not

improve the GVL selectivity (71%), though it did produce additional hydrogenation products, e.g., 20% 1,4-PDO and 8–9% pentane.

3.2.2. Effect of FA concentration on LA hydrogenation

The FA concentration used to selectively obtain GVL was changed by changing the LA to FA molar ratio in the feed over Ni(8)Cu(72)-SiO_2 catalyst (Table 5). The LA to FA molar ratios of 1:1, 1:2, and 1:3 were tested in the comparison study. LA conversion and GVL selectivity increased with increasing FA concentration in the feed. The highest LA conversion of 97% and GVL selectivity of 98% were obtained with 1:3 LA to FA molar ratio (Table 5). We also performed the experiment using a higher concentration of FA (i.e., 1:10) to check further possibilities. Not surprisingly, the GVL selectivity (79%) decreased with higher FA concentration, and additional hydrogenation products were created (15% 1, 4-PDO and 3% MTHF). For comparison, we conducted synthesis of GVL over Ni(20)Cu(60)-SiO_2 catalyst using 1:0.5 LA to FA molar ratio in the feed. This combination afforded poor LA conversion and poor GVL selectivity compared to 1:1 molar ratio of LA to FA. In this case, AL was the major product instead of GVL. However, the highest GVL yield from LA (98%) was obtained using Ni(20)Cu(60)-SiO_2 and 1:2 LA to FA molar ratio in the feed.

3.2.3. Effect of reaction temperature on LA hydrogenation

From the study above, the molar ratios of 1:3 and 1:2 (of LA to FA) are optimum to obtain GVL selectively under the reaction conditions given in Table 6 for Ni(8)Cu(72)-SiO_2 and Ni(20)Cu(60)-SiO_2 catalysts, respectively. However, it should be noted that LA and FA are always obtained in the 1:1 (molar) proportion because of the decomposition of hexose sugar [4]. By considering this, a further study was carried out using 1:1 molar ratio of LA/FA in the feed. The effect of different reaction temperatures on the activity of the catalyst is presented in Table 6. At the lower reaction temperature of 240 °C, the LA conversion and GVL selectivity were lower compared to those obtained with higher reaction temperatures. The selective conversion of 73% of the LA to 67% GVL was obtained using Ni(8)Cu(72)-SiO_2 catalyst. It also provided an intermediate A-lactone selectivity of 31% at 240 °C. At the same temperature, the catalyst [Ni(20)Cu(60)-SiO_2] yielded 78% GVL and 21% A-lactone with 90% conversion of LA. The catalytic activities of both the catalysts were greater at higher reaction temperatures. The highest LA conversion (99%) and GVL selectivity (96%) were obtained at the reaction temperature of

285 °C with the Ni(20)Cu(60)-SiO_2 catalyst. The second best results were obtained using 8% of nickel Ni(8)Cu(72)-SiO_2 catalyst at 285 °C, and this combination yielded converted 92% LA into 88% GVL. However, this temperature is very close to the Tamman temperature of copper, which is considered the point at which sintering begins in the metal species. A marginal difference in activity was observed for the top two catalysts at 265°C compared to that obtained at 285°C for hydrogenation of LA.

3.2.4. Long-term activities of Ni-promoted Cu-SiO_2 catalysts

To check the stability of the Ni-promoted Cu-SiO_2 nanocomposite catalysts, we conducted catalytic measurements as a function of reaction time. The time-on-stream profiles for the Ni(8)Cu(72)-SiO_2 and Ni(20)Cu(60)-SiO_2 catalysts are presented in Figure 8. In the case of the former catalyst, the initial LA conversion was found to be 87–90% with 86% GVL, after up to 100 h of reaction. After 100 h of reaction, a marginal decrease in the LA conversion (83%) and GVL selectivity (82%) was observed; 15–19% selectivity for AL was also observed (Figure 6). It is clear that the Ni(20)Cu(60)-SiO_2 catalyst exhibited excellent performance and longer stability (200 h) without deactivation. Furthermore, it yielded 92% GVL selectively with 98% conversion of LA in LA hydrogenation using formic acid as a hydrogen source.

4. Conclusions

The highly dispersed Ni-promoted Cu-SiO_2 nanocomposite catalysts provide excellent catalytic activity for hydrogenation of biomass-derived LA (using FA as the hydrogen source) to selectively produces GVL. The addition of Ni to Cu-loaded catalysts enhances the thermal stability, conforming through the excellent catalytic results obtained at 285 ^{o}C without any deactivation, and more importantly, the nanocomposite nature of catalysts could also helps to prevents Cu sintering even after long reaction time after 200 h of reaction time. The current catalyst system has shown its efficient and steady workability for the carboxylic acid hydrogenation continuously in vapor phase. Therefore, Ni-promoted Cu-SiO_2 catalysts would be considered a promising candidate of catalysts for hydrogenation of LA to GVL without metal leaching. Hence, the current finding seems to be more affordable and allows us to think about the synthesis of value added chemicals *via* hydrogenation of biomass derived platform chemicals without any external hydrogen

Acknowledgements

This work was supported by the Institutional Research Program (KK-1401-F0) and partly by from the Korea Research Council for Industrial Science and Technology (ISTK, SK-1411). The authors thank Mr. K.-H. Cho and Ms. S.-K. Lee for their beneficial contributions.

References

[1] J. Yan, P. Alvfors, L. Eidensten, G. Svedberg. A future for biomass, by the American Society of Mechanical Engineers**, 1997,** *119*, 94-96.

[2] a) G.W. Huber, S. Iborra, A. Corma, Chem. Rev. **2006**, *106*, 4044-4098; b) A. S. Mamman, J. M. Lee, Y. C. Kim, I. T. Hwang, N.J Park, Y. K. Hwang, J. S. Hwang, J.S . Chang, Biofuel. Bioprod. Bioref. **2006**, *2***,** 438-454.

[3] a) M. G. Al-Shaal, W. R. H. Wright, R. Palkovits, Green Chem. **2012**, *14*, 1260-1263; b) A. M. Raspolli Galletti, C. Antonetti, V. D. Luise, M. Martinelli, Green Chem. 2012, 14, 688-694; c) E. C. Douglas, US patent 5883266, **1999**.

[4] a) P. P. Upare, J.-W. Yoon, M. Y. Kim, H.-Y. Kang, D. W. Hwang, Y. K. Hwang, H. H. Kung, J.-S. Chang, Green Chem. **2013**, 15, 2935–2943; b) D. J. Hayes, S. Fitzpatrick, M. H. B. Hayes, J. R. H. Ross in Biorefineries: Industrial Processes and Products, Vol. 1 (Eds: B. Kamm, P. R. Gruber, M. Kamm), Wiley-VCH, Weinheim**, 2006,** pp. 139-164;c) D. W. Rackemann, W. O. S. Doherty, Biofuels, Bioprod. Bioref**. 2011***, 5***,**198-214.

[5] a) X. L. Du, Q.Y. Bi, Y. M. Liu, Y. Cao, H. Y. He, K. N. Fan, Green Chem. **2012,** *14*, 935-939 ;b) L.E. Manzer, US patent, 6,617,464 B2, **2003**; c) L.E. Manzer, K. W. Hutchenson, US Patent, 6,946,563B2, **2005.**

[6] J. Q. Bond, D. M. Alonso, D. Wang, R. M. West, J. A. Dumesic, Science**, 2010***, 327***,** 1110-1114.

[7] a) R. W. Christian, H.D. Brown, R.M. Hixon, J. Am. Chem. Soc. **1947**, *69*, 1961-1963; b) H. A. Schuette, R. W. Thomas, J. Am. Chem. Soc. **1930**, *52*, 3010 - 3012; c) L. E. Manzer, Appl. Catal. A: Gen. 2004, *272*, 249 - 256; d) J. J. Bozell, L. Moens, D. C. Elliott, Y. Wang, G. G Neuenscwander, S. W Fitzpatrick, R. J Bilski, J. L Jarnefeld, Resources Conv. Recycl**. 2000**, *28*, 227-239; e) W. A. Farone, J. E. Cuzens, US patent 6054611, **2000**; f) P. P. Upare, J. M. Lee, D. W. Hwang, S. B. Halligudi, Y. K. Hwang, J.-S. Chang. J. Ind. Eng. Chem**. 2011**, *17*, 287-292; g) A. M. Hengne, C. V. Rode**,** Green Chem. **2012**,*14*, 1064-1072.

[8] a) F. M. A. Geilen, B. Engendahl, A. Harwardt, W. Marquardt, J. Klankermayer, W. Leitner, Angew. Chem. Int. Ed. **2010**, *49*, 5510 -5514; b) R. A. Bourne, J. G. Stevens, J. Ke, M. Poliakoff, Chem. Commun. **2007**, 4632- 4634.

[9] a) L. Deng, J. Li, D. M. Lai, Y. Fu, Q. X. Guo , Angew. Chem. Int. Ed. 2009, *48*, 6529 - 6532; b) L. Deng, Y. Zhao, J. Li, Y. Fu, B. Liao, Q. X. Guo, ChemSusChem **2010**, *3*, 1172-1175.

[10] X. L. Du, L. He, S. Zhao, Y. M. Liu, Y. Cao, H. Y. He, K. N. Fan, Ang. Chem. Int. Ed. **2011**, *50*, 7815-7819.

[11] H. Heeres, R. Handana, D. Chunai, C. B. Rasrendra, B. Girisuta, H. J. Heeres, Green Chem. **2009**, *11*, 1247-1255.

[12] D. J. Braden, C. A. Henao, J. Heltzel, C. C. Maravelias, James A. Dumesic, Green Chem. **2011**, 13, 1755-1765.

[13] A. Yin, C. Wen, X. Guo, W. L. Dai , K. Fan, J. Catal. **2011**, *280*,77-88.

[14] a) P. G. Menon, *Chem. Rev.* **1994**, *94*, 1021- 1046; b) C. I. Meyer, A. J. Marchi, A. Monzon, T. F. Garetto, Appl. Catal. A: Gen. **2009**, *367*,122-129.

[15] P. P. Upare, J. M. Lee, Y. K. Hwang, D. W. Hwang, J. H. Lee, S. B. Halligudi, J. S. Hwang, J. S. Chang, ChemSusChem, **2011,** *4*, 1749-1752.

[16] K.J. Carroll, J.U. Reveles, M.D. Shultz, S.N. Khanna, E. E. Carpenter, J. Phys. Chem. C, **2011**, *115*, 2656-2664.

[17] S. A. Khromova, A. A. Smirnov, O .A. Bulavchenko, A. A. Saraev, V. V. Kaichev, S. I. Reshetnikov, V. A. Yakovlev, Appl. Catal. A: Gen. 2014, 470, 261-270

[18]I. Kasatkin, P. Kurr, B. Kniep, A. Trunschke, R. Schlgl, Angew. Chem. **2007**, *119*, 7465-7468.

[19] a) B. R. Strohmeier, D. E. Levden, R. S. Field, D. M. Hercules, J. Catal. 1985, 94, 514–530; b) S. Poulston, P. M. Parlett, P. Stone, M. Bowker, Surf. Interface Anal. 1996, 24, 811–820; c) J. Batista, A. Pintar, D. Mandrino, M. Jenko, V. Martin, Appl. Catal. A 2001, 206, 113–124. d) M. C. Biesinger, L.W.M. Lau, A. R. Gerson, R. St. C. Smart, Appl. Surf. Sci. 2010, 257, 887–898

[20] M. V. Bykova, D. Yu. Ermakov, V. V. Kaichev, O. A. Bulavchenko, A. A. Saraev, M. Yu. Lebedev, V. A. Yakovlev, Appl. Catal. A:Gen. 2012, 113-114, 296-307.

[21] a) N. S. McIntyre, M. G. Cook, Anal. Chem. 1975, 47, 2208–2213; b) C. P. Li, A. Proctor, D. M. Hercules, Appl. Spectrosc. 1984, 38, 880–886; c) C. E. Dube, B. Workie, S. P. Kounaves, A. Rabbat, M. L. Aksu Jr., G. Davies, J. Electrochem. Soc. 1995, 142,

3357–3365; d) N. V. Kosova, E. T. Devyatkina, V. V. Kaichev, J. Power Sources 2007, 174, 735–740.

[22] a) R. B. Shalvoy, P. J. Reucroft, J. Catal. 1979, 56, 336–348; b) M. L. Occelli, D. Psaras, S. L. Suib, J. M. Stencel, Appl. Catal. 1986, 28, 143–160; c) P. Lorenz, J. Finster, G. Wendt, J. V. Salyn, E. K. Zumadilov, V. I. Nefedov, J. Electron Spectrosc. Relat. Phenom. 1979, 16, 267–276.

[23] A. R. Naghash, T. H. Etsell, S. Xu, Chem. Mater. **2006**, *18*, 2480-2488.

[24] a) P. P. Florez-Rodriguez, A. J. Pamphile-Adrián, F. B. Passos, Catalysis Today, 2014, dx.doi.org/10.1016/j.cattod.2013.12.026; b) A. Loaiza-Gil, M.Villarroel, J. F. Balbuena, M. A. Lacruz, S. Gonzalez-Cortes, J. Mol. Cat. A: Chem. 2008, 281, 207-213, c) F. Frusteria, S. Frenia, V. Chiodoa, S. Donatoa, G. Bonuraa, S. Cavallaro, International Journal of Hydrogen Energy 2006, 31, 2193 -2199; d) M. Kang, M. W. Song, T. W. Kim, K. L. Kim, The Canadian Journal of Chemical Engineering, 2008, 80, 63-70.

[25] A. R. Naghash, T. H. Etsell, S. Xu, Chem. Mater. 2006, 18, 2480-2488.

[26] G. W. Huber, J. W. Shabakar, J. A. Dumesic, *Science*, **2003**, *300*, 2075-2077.

Table 1. H_2 chemisorptions of Cu-SiO_2 and Ni-promoted Cu-SiO_2 catalysts

Catalyst	Metallic Surface Area (m^2/g)		H_2 Uptake (mmol/g)	Total Dispersion (%)	
	Cu	Ni		Cu	Ni
Cu(80)-SiO_2	4.26	0	0.030	0.82	0
Ni(8) Cu(72)-SiO_2	3.05	1.06	0.035	0.58	0.41
Ni(20)Cu(60)-SiO_2	2.10	1.51	0.039	0.55	0.45
Ni(40)Cu(40)-SiO_2	6.56	5.30	0.130	2.04	2.11

Table 2. ICP analysis of Cu-SiO_2 and Ni-promoted Cu-SiO_2 catalysts.

Catalyst	SiO_2	CuO	NiO
	Atomic %	Atomic %	Atomic %
Cu(10)/SiO_2	88.25	9.62	-
Cu(80)-SiO_2	26.1	73.9	-
Ni(4)Cu(76)/SiO_2	26.4	71.36	3.14
Ni(8)Cu(72)-SiO_2	26.8	66.2	7.0
Ni(20)Cu(60)-SiO_2	24.4	58.8	16.8
Ni(30)Cu(50)-SiO_2	21.18	47.8	30.03
Ni(40)Cu(40)-SiO_2	22.3	36.1	38.2

Table 3. Atomic ratio of Cu-SiO_2 and Ni-promoted Cu-SiO_2 catalysts from XPS analysis.

Catalyst	Si	Cu	Ni
	Atomic % Reduction (Calcination)	Atomic % Reduction (Calcination)	Atomic % Reduction (Calcination)
Cu(80)-SiO_2	54.1(53.8)	45.9(46.2)	-
Ni(8)Cu(72)-SiO_2	44.8(44.3)	43.4(44.2)	11.8(11.5)
Ni(20)Cu(60)-SiO_2	40.3(41.1)	44.0(43.5)	14.7(15.4)

Table 4. Catalytic activities for hydrogenation of levulinic acid using FA as H_2 source.

Catalyst	S_{BET} (m^2/g)	Conv. (%)	Selectivity (%)[a]		TOF
			AL	GVL	
Cu(10)-SiO_2	291	66	55	40	1.72
Cu(80)-SiO_2	142	83	19	81	0.28
Ni(4)Cu(76)-SiO_2	160	85	18	82	0.29
Ni(8) Cu(72)-SiO_2	166	88	12	88	0.30
Ni(20)Cu(60)-SiO_2	214	98	8	92	0.32
Ni(20)Cu(60)-SiO_2[b]	214	96	11	89	0.32
Ni(30)-Cu(50)-SiO_2 [c]	202	100	0	81	0.31
Ni(40)Cu(40)-SiO_2[d]	193	100	0	71	0.32

*Reaction conditions: Temp. of 265^{o}C, LA: FA of 1:1 (molar ratio), Feed 10% in 1,4-dioxane, Nitrogen flow of 20ml/min, Catalyst wt. of 1gm, Acid WHSV of 0.512 h^{-1}, Pressure of 1 atm., TOS of 100 h. TOF= (Reacted mole of LA)/Total mole of metals (Cu-Ni) per hour

[a]Abbreviation: AL, angelica lactone; GVL, γ-valerolactone.

[b]Reaction was carried out using mixture of H_2 and CO_2 as a hydrogen source instead of FA, (i.e. LA: hydrogen =1:1 molar ratio).

[c]Other products include 1,4-PDO (13-14%) and pentane (4-5%).

[d]Other products include 1,4-PDO (20%) and pentane (8-9%).

*

Table 5. Effect of different molar ratio of LA/FA on catalytic activity.

Catalyst	Molar ratio of LA/FA	Conversion (%)	Selectivity (%)	
			A- lactone	GVL
Ni(8)Cu(72)-SiO_2	1	90	12	86
	0.5	93	3	96
	0.33	97	2	98
	0.1[a]	100	-	79
Ni(20) Cu(60)-SiO_2	2	87	47	45
	1	98	8	92
	0.5	100	2	98

Reaction conditions: Temperature 265 ^{o}C, pressure = 1 bar, Nitrogen flow 20 ml/min, Catalyst wt. = 1.0 gm, Acid WHSV = 0.512 h^{-1}, pressure = 1 atm, TOS = 100h

[a]Other products include 1,4-pentanediol (15%), MTHF (3%), hydrocarbons (3%) such as pentane, CO and CO_2. *The concentration of LA (7.2 g) was kept constant and concentration of formic acid was varied accordingly

Table 6. Effect of reaction temperature on catalytic activity.

Catalyst	Temp. (^{o}C)	Conv. (%)	Selectivity (%)	
			AL	GVL
Ni(8)Cu(72)-SiO_2	240	73	31	67
	265	90	12	86
	285	92	9	88
Ni(20)Cu(60)-SiO_2	240	90	21	78
	265	98	8	92
	285	99	3	96

Reaction conditions: LA: FA= 1:1 (molar ratio), N_2 flow 20 ml/min, catalyst wt. = 1.0 gm, Acid WHSV = 0.512 h^{-1}, pressure = 1 atm, TOS-100 h.

Figure captions

Figure 1. XRD patterns of calcined Cu-Ni catalysts at 550°C for 8h. (a) Cu(80)-SiO_2, (b) Ni(8)Cu(72)-SiO_2, (c) Ni(20)Cu(60)-SiO_2, (d) Ni(30)Cu(60)-SiO_2, and (e) Ni(40)Cu(40)-SiO_2.

Figure 2. XRD patterns of reduced Cu-Ni catalysts at 290°C with a mixture of 5% H_2 in N_2 for 2h. (a) Cu(80)-SiO_2, (b) Ni(8)Cu(72)-SiO_2, (c) Ni(20)Cu(60)-SiO_2, (d) Ni(30)Cu(50)-SiO_2, (e) Ni(40)Cu(40)-SiO_2, and (f) Ni(80)/SiO_2

Figure 3. XRD patterns of used Cu-Ni catalysts after hydrogenation of 200 h. (a) Cu(80)-SiO_2, (b) Ni(8)Cu(72)-SiO_2, (c) Ni(20)Cu(60)-SiO_2, (d) Ni(30)Cu(60)-SiO_2, and (e) Ni(40)Cu(40)-SiO_2.

Figure 4. TEM images of catalysts: (a) Ni(8)Cu(72)-SiO_2 (reduced), (b) Ni(8)Cu(72)-SiO_2 (used), (c) Ni(20)Cu(60)-SiO_2 (reduced), (d) Ni(20)Cu(60)-SiO_2 (used) and (e) HR-TEM of reduced Ni(8)Cu(72)-SiO_2 catalyst. The calcined catalysts were reduced at 290°C for 2 h under 5% H_2 in inert gas, and then were used for the hydrogenation for 200 h.

Figure 4. TEM-EDS mapping images of the reduced Ni(20)Cu(60)-SiO_2 catalyst.

Figure 5. X-ray photoelectron spectra of calcined and reduced catalysts for Cu-SiO_2 and NiCu-SiO_2: (a) Cu 2p and (b) Ni 2p spectra of the calcined catalysts. (c) Cu 2p and (d) Ni 2p spectra of the reduced catalysts, respectively.

Figure 6. X-ray photoelectron spectra of calcined and reduced catalysts for Cu-SiO_2 and NiCu-SiO_2: (a) Cu 2p and (b) Ni 2p spectra of the calcined catalysts. (c) Cu 2p and (d) Ni 2p spectra of the reduced catalysts, respectively.

Figure 7. TPD profiles of Cu-SiO_2 and NiCu-SiO_2 catalysts: (a) Cu(80)-SiO_2, (b) Ni(8)Cu(72)-SiO_2, and (c) Ni(20)Cu(60)-SiO_2.

Figure 8. Catalytic activities on stream for hydrogenation of levulinic acid: (a) Ni(8)Cu(72)-SiO_2 and (b) Ni(20)Cu(60)-SiO_2 catalysts. Reaction conditions: Temperature of 265°C, LA: FA of 1:1 (molar ratio), Nitrogen flow of 20ml/min, Feed of 10 % in 1, 4-dioxane, Catalyst weight of 1g, Acid WHSV of 0.512 h^{-1}, and pressure of 1 atm.

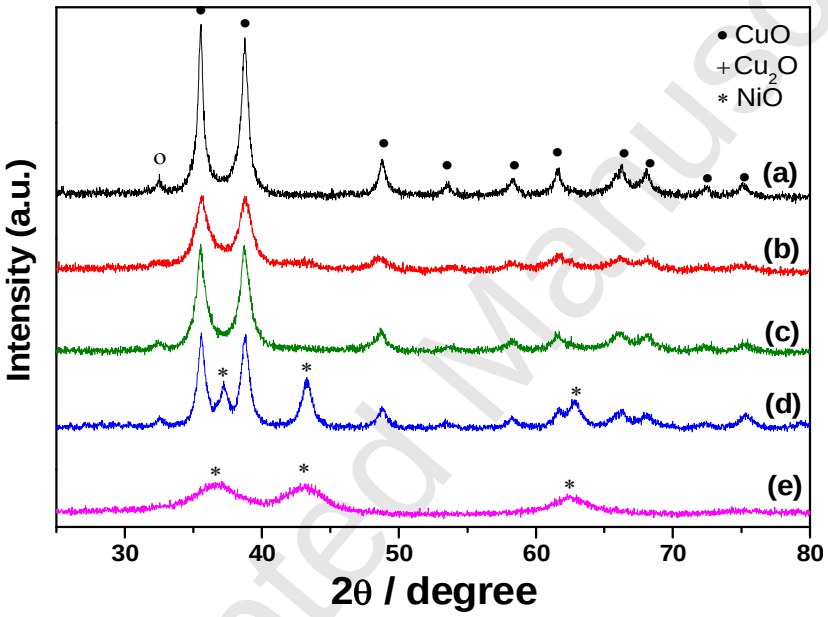

Figure 1. XRD patterns of calcined Cu-Ni catalysts at 550°C for 8h. (a) Cu(80)-SiO_2, (b) Ni(8)Cu(72)-SiO_2, (c) Ni(20)Cu(60)-SiO_2, (d) Ni(30)Cu(60)-SiO_2, and (e) Ni(40)Cu(40)-SiO_2.

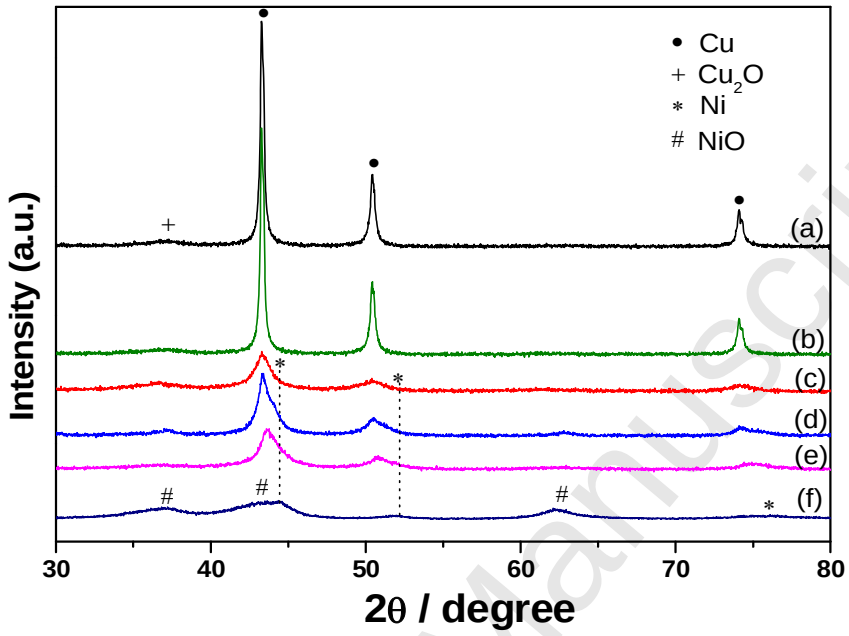

Figure 2. XRD patterns of reduced Cu-Ni catalysts at 290°C with a mixture of 5% H_2 in N_2 for 2h. (a) Cu(80)-SiO_2, (b) Ni(8)Cu(72)-SiO_2, (c) Ni(20)Cu(60)-SiO_2, (d) Ni(30)Cu(50)-SiO_2, (e) Ni(40)Cu(40)-SiO_2, and (f) Ni(80)/SiO_2.

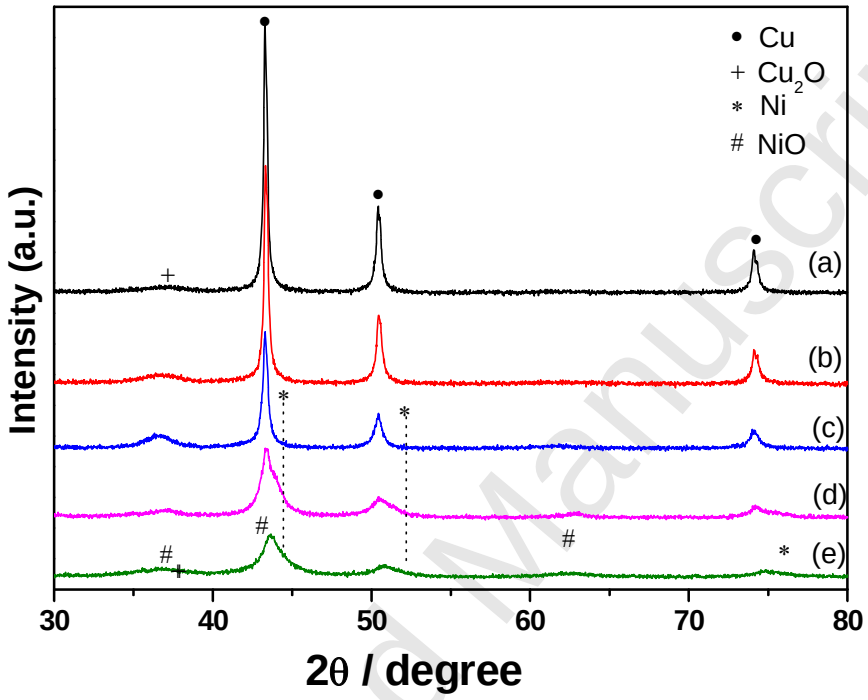

Figure 3. XRD patterns of used Cu-Ni catalysts after hydrogenation of 200 h. (a) Cu(80)-SiO_2, (b) Ni(8)Cu(72)-SiO_2, (c) Ni(20)Cu(60)-SiO_2, (d) Ni(30)Cu(60)-SiO_2, and (e) Ni(40)Cu(40)-SiO_2.

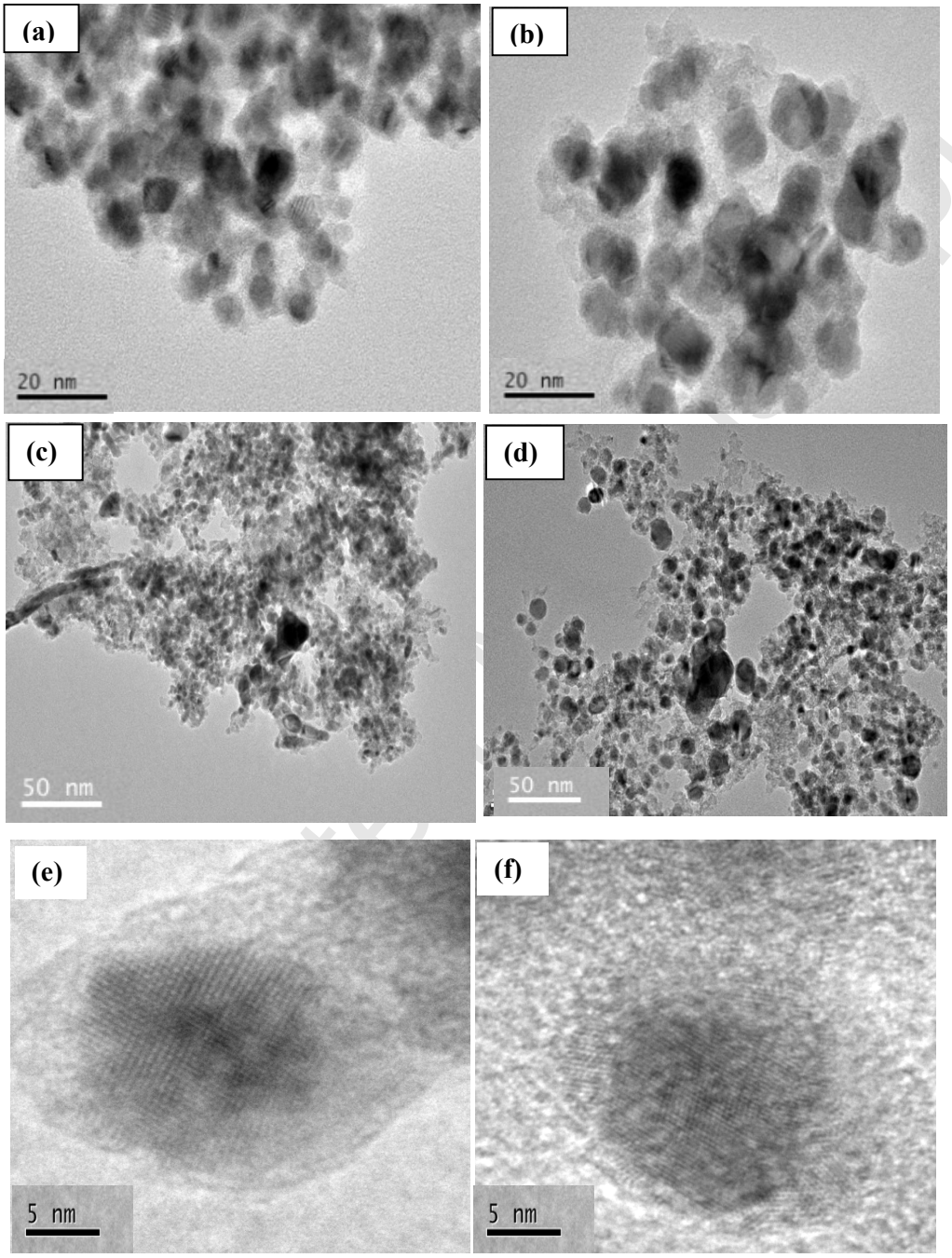

Figure 4. TEM images of catalysts: (a) Ni(8)Cu(72)-SiO_2 (reduced), (b) Ni(8)Cu(72)-SiO_2 (used), (c) Ni(20)Cu(60)-SiO_2 (reduced), (d) Ni(20)Cu(60)-SiO_2 (used), (e) and (f) HR-TEM of reduced Ni(8)Cu(72)-SiO_2 ((100) and (111) plane of Cu nanoparticles, respectively). The calcined catalysts were reduced at 290^{o}C for 2 h under 5% H_2 in inert gas, and then were used for the hydrogenation for 200 h.

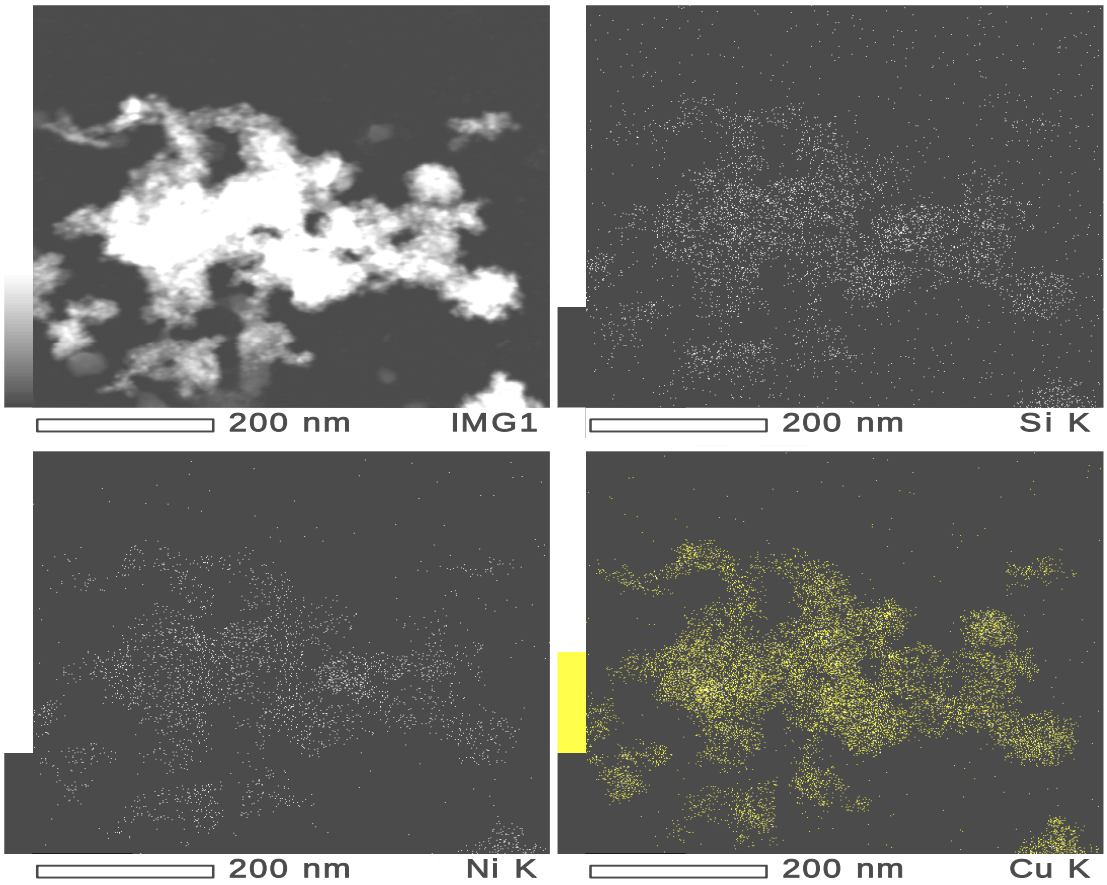

Figure 5. TEM-EDS mapping images of the reduced Ni(20)Cu(60)-SiO_2 catalyst.

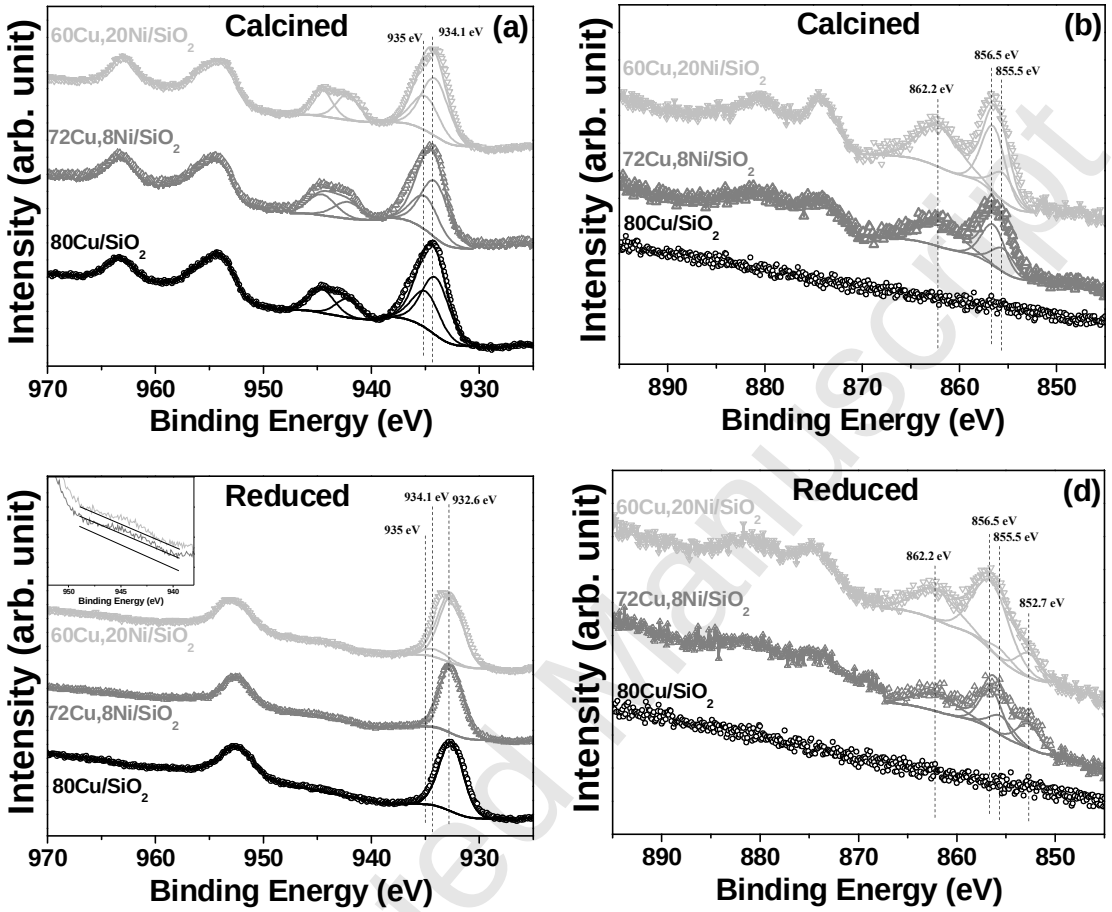

Figure 6. X-ray photoelectron spectra of calcined and reduced catalysts for Cu-SiO_2 and NiCu-SiO_2: (a) Cu 2p and (b) Ni 2p spectra of the calcined catalysts. (c) Cu 2p and (d) Ni 2p spectra of the reduced catalysts, respectively.

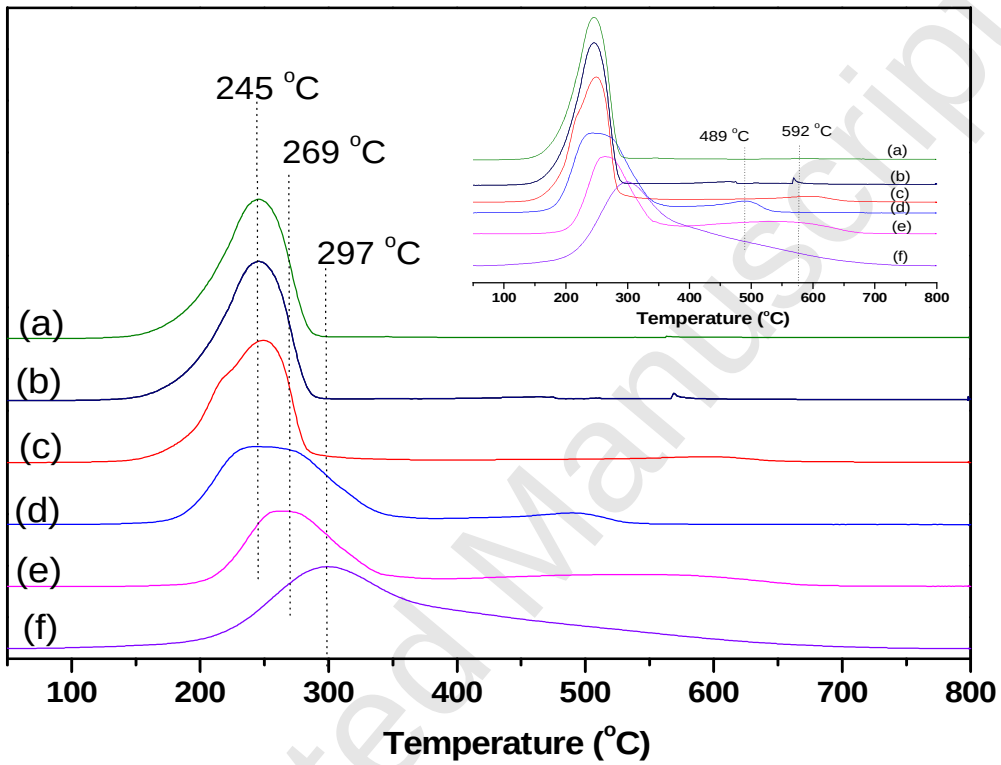

Figure 7. TPR profiles of Cu-SiO_2 and NiCu-SiO_2 catalysts: (a) Cu(80)-SiO_2, (b) Ni(8)Cu(72)-SiO_2, (c) Ni(20)Cu(60)-SiO_2, (d) Ni(30)Cu(50)/SiO_2, (e) Ni(40)Cu(40)/SiO_2, and (f) Ni(80)/SiO_2. * TPR of Ni(80)/SiO_2 is used here as a references

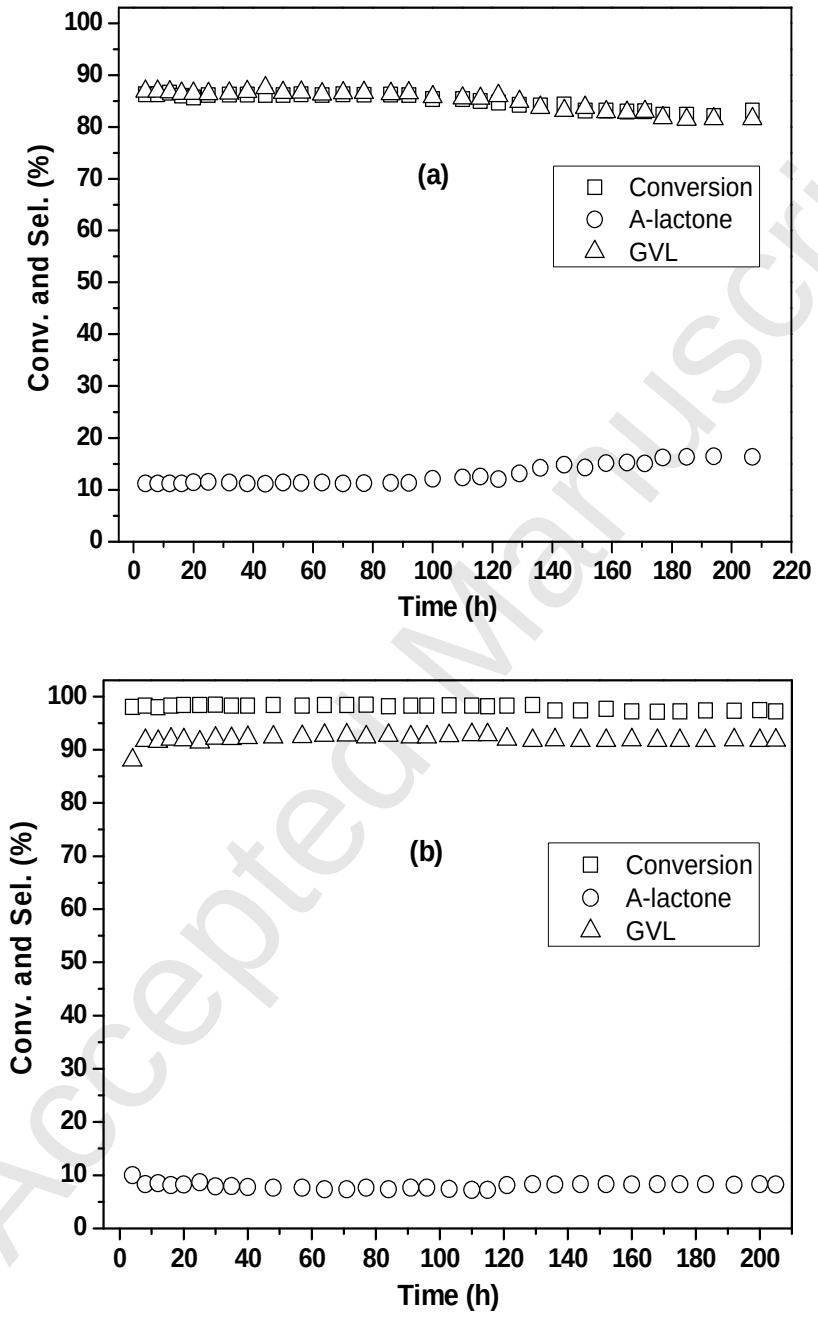

Figure 8. Catalytic activities on stream for hydrogenation of levulinic acid: (a) Ni(8)Cu(72)-SiO_2 and (b) Ni(20)Cu(60)-SiO_2 catalysts. Reaction conditions: Temperature of 265^{o}C, LA: FA of 1:1 (molar ratio), Nitrogen flow of 20ml/min, Feed of 10 % in 1, 4-dioxane, Catalyst weight of 1g, Acid WHSV of 0.512 h^{-1}, and pressure of 1 atm.

Highlights

- Levulinic acid hydrogenation using formic acid as H_2 source studied over Ni-Cu/SiO_2.
- Ni(20)-Cu(60)/SiO_2 continuously produced γ-valerolactone with 97% yield.
- Ni-Cu/SiO_2 shown its stability up to 200 h without any loss of catalytic activity.
- Metallic dispersion in Ni-Cu/SiO_2 is mainly responsible for superior catalytic activity.

Graphical Abstract

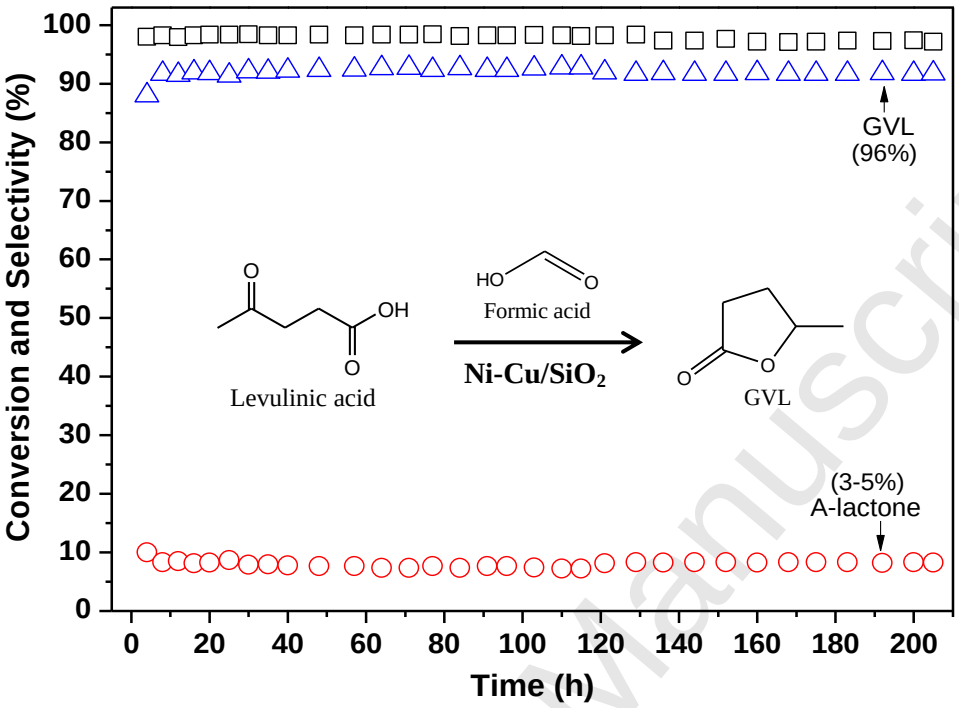

Continuous hydrogen free hydrogenation of biomass derived Levulinic acid to GVL